

NOTICE CONCERNING COPYRIGHT RESTRICTIONS

This document may contain copyrighted materials. These materials have been made available for use in research, teaching, and private study, but may not be used for any commercial purpose. Users may not otherwise copy, reproduce, retransmit, distribute, publish, commercially exploit or otherwise transfer any material.

The copyright law of the United States (Title 17, United States Code) governs the making of photocopies or other reproductions of copyrighted material.

Under certain conditions specified in the law, libraries and archives are authorized to furnish a photocopy or other reproduction. One of these specific conditions is that the photocopy or reproduction is not to be "used for any purpose other than private study, scholarship, or research." If a user makes a request for, or later uses, a photocopy or reproduction for purposes in excess of "fair use," that user may be liable for copyright infringement.

This institution reserves the right to refuse to accept a copying order if, in its judgment, fulfillment of the order would involve violation of copyright law.

Injection Testing for an Enhanced Geothermal System Project at Desert Peak, Nevada

S. K. Sanyal¹, J. W. Lovekin¹, R. C. Henneberger¹, A. Robertson-Tait¹,
P. J. Brown¹, C. L. Morris² and D. Schochet²

¹GeothermEx, Inc.
²ORMAT Nevada, Inc.

Keywords

Desert Peak, Enhanced Geothermal System, EGS, HDR, injection, stimulation, formation evaluation, well testing, injectivity, flow capacity, storage capacity, skin factor, vertical fracture

ABSTRACT

An Enhanced Geothermal System (EGS) project, partially funded by the U.S. Department of Energy, is under development at the Desert Peak field in Nevada. For this project, an existing non-commercial well (DP 23-1), to be stimulated by hydraulic fracturing, has been the subject of various recent investigations. One focus of this work has been an evaluation of the existing network of fractures in the well via acquisition of a wellbore-imaging log, which required cooling the wellbore (by water injection) to ensure good image quality. This cooling effort provided an opportunity to conduct an injection test of the well.

A step-rate injection test and a pressure fall-off test, following the stoppage of injection, were conducted. The injection rate and pressure data were analyzed using transient pressure analysis techniques. This analysis confirmed that the reservoir around the well has very low flow capacity (4,000 md-ft) and a modest storage capacity (0.001 ft/psi), and the well does not intersect any major fracture. The well has very low injectivity (0.69 gpm/psi). The analysis indicates that injection for several days reduced the wellbore "skin factor" (from 1 to -0.2), and thereby, improved the injectivity somewhat. The positive skin factor of this well appears to be due to possible well damage and the fact that less than half of the open interval in the well accepts injection. The average porosity of the reservoir is very low (on the order of 2%). The radius of investigation of the test was estimated at 1,440 feet. The flow and storage capacities at this well are far lower than encountered within the known hydrothermal reservoir at Desert Peak.

The results of this test provide a baseline against which any future permeability enhancements at this well can be assessed; a practical, low cost and approximate methodology for such assessment is proposed. The methodology consists of a short-term injection test followed by a long-term test (several weeks) that

will yield the following measures of stimulation success: increase in injectivity, flow capacity and/or fracture length; reduction in skin factor; and stimulated reservoir volume.

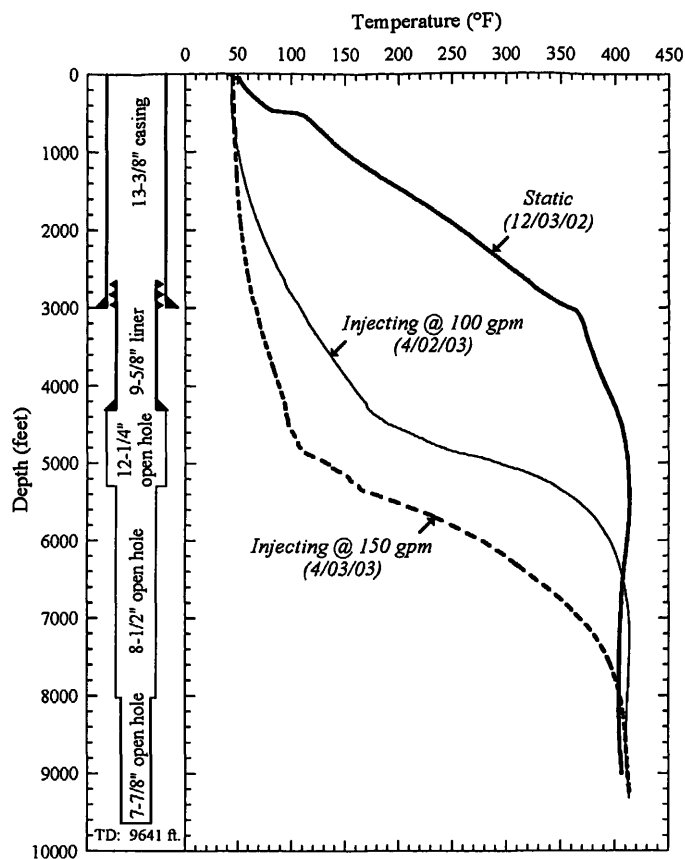
Introduction

Ormat Nevada Inc. has received funding from the U.S. Department of Energy on a cost-shared basis to investigate the technical and economic feasibility of creating an artificial geothermal reservoir on the eastern flank of the Desert Peak geothermal field. This project has the ultimate goal of developing 2 to 5 MW of EGS-derived power from a stand-alone binary power plant supplied by 2 to 4 wells. Focusing initially on existing well DP 23-1, a hot but tight hole about 1.5 miles east of the producing hydrothermal wells, a systematic Phase I evaluation of the EGS potential of this area is underway (Robertson-Tait and Morris, 2003).

One major task in Phase I is evaluation of the stress field in the vicinity of well DP 23-1, and an analysis of the existing fracture population in the open-hole portion of the well via acquisition and interpretation of a wellbore-imaging log. This log will also indicate whether the well encounters fractures optimally oriented to fail in shear; such fractures are likely to remain open, and therefore, would be favorable for creating an artificial geothermal reservoir around the well using hydraulic stimulation techniques. Acquisition of the log required cooling the wellbore by water injection to ensure good image quality. This cooling effort provided an opportunity to conduct an injection test. The test design included a step-rate injection test and a pressure fall-off test at the end of the injection period, both with downhole pressure monitoring. Periodic temperature surveys were run during the cooling/testing period to evaluate how the cool-down was proceeding.

Injection and Logging Operations

The completion of the well and temperature surveys taken at various times are shown in Figure 1. Well DP 23-1 was originally drilled in 1979 to a depth of 9,641 feet. A sinker-bar run in December 2002 showed the wellbore to be open to a depth of 9,600 feet, and a temperature-pressure-spinner (TPS) log confirmed the



2003, GeothermEx, Inc.

Figure 1. Well 23-1 completion and temperature logs.

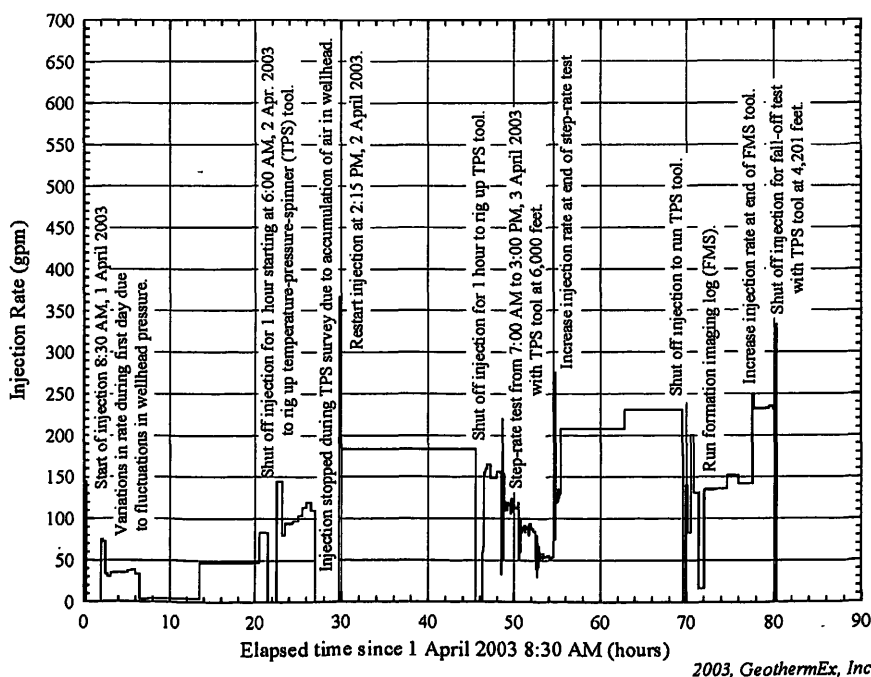
results of historical temperature surveys (Figure 1). The recent logging and testing program comprised the following activities over 4 days: three TPS logs, a step-rate injection test, a gamma-ray log, a wellbore-imaging log, and a pressure-fall-off test.

The injection water was pumped in from the cooling tower at the Desert Peak power plant, located about 2 miles away. The wellhead was configured with a flow tee equipped with a pressure gauge and a thermometer; a flow-control valve was mounted on the inlet to the tee. Injection rates were metered with an impeller meter installed on the injection line. Injection began on 1 April; Figure 2 shows the injection rate as a function of elapsed time, with annotations about significant changes in injection operation. The first TPS log reached 400°F at 6,182 feet on the down run and measured a maximum temperature of 413°F on bottom, tagged at 9,310 feet. This indicated a loss of 290 feet of open-hole interval since the sinker bar was run in December 2002, possibly due to sloughing of the well in response to the thermal stress of the first day of injection. With the TPS tool at 8,220 feet on the down run, the well stopped taking injection, apparently due to an accumulation of air in the wellhead. The remainder of the log

was conducted with no injection. Toward the end of the up run, the air was bled off the wellhead, and injection resumed after the TPS tool was out of the hole.

The step-rate test was conducted on 3 April using the TPS tool to measure downhole pressures, with the wellhead on vacuum. With an injection rate of 150 gallons per minute (gpm), the TPS tool was initially run to bottom, measuring the complete temperature profile. The tool reached 400°F at 7,820 feet (1,638 feet deeper than the down run on the previous day), but the temperature at bottom (tagged at 9,281 feet, 29 feet shallower than the day before) was unchanged at 413°F. The tool was then pulled up to 6,000 feet. During the step-rate test, the injection rate was reduced in three steps of 2 hours duration each: 120, 90, and 60 gpm. Flow rates were measured using both the needle indicator and the totalizer on the flow meter. The needle indicator was used to set the position of the flow-control valve for each rate step, but it proved unreliable, reading 20 gpm lower than the rates calculated from the totalizer. The rates cited above and the data analysis discussed below were based on the totalizer readings. After the step-rate test, the flow-control valve was opened up, and injection spiked to 700 gpm before settling down to 130 gpm. Monitoring of pressures at 6,000 feet continued for another 50 minutes. The TPS tool was then pulled out of the hole and the injection rate was maximized to aid the cool-down of the wellbore. The wellbore imaging log was successfully run while maintaining injection at 140 gpm.

The pressure fall-off test was conducted after completion of wellbore imaging logging. Prior to the fall-off test, the injection rate was increased to 230 gpm. The wellhead remained on vacuum, and the top valve on the wellhead was left open. With the TPS tool set at a depth of 4,201 feet, injection was shut off and pressure fall-off monitored for 4.5 hours. The top valve on the wellhead remained open throughout the fall-off test.



2003, GeothermEx, Inc.

Figure 2. Desert Peak 23-1 injection test: rate step history.

Analysis of Injection Test Data

Analysis Methodology

Analyses of the wellbore imaging, TPS and gamma-ray logs run during the test are underway; only the analysis of the injection test results are reported below. The injection rate data were treated as a series of rate steps (Figure 2) with a total of 4,300 steps being considered for analysis. For each rate step, the bottom-hole pressure was calculated by an analytical modeling approach. This approach superimposes, in time, a solution of the diffusivity equation describing the pressure distribution in the reservoir. Two alternative solutions were considered:

1. the “line source solution” (Earlougher, 1977) representing injection into a well in a purely porous medium and including the skin factor (an index of wellbore flow efficiency); and
2. the “uniform flux” vertical fracture solution (Gringarten *et al.*, 1975) representing injection into a well intersecting a vertical fracture in a porous medium.

Considering each solution in turn and superimposing the solution in time (for the 4,300 rate steps), the pressure behavior of the well was calculated for the entire 80-hour test period. In addition to the rate steps, the other input parameters for this calculation are: initial wellbore pressure, reservoir fluid viscosity and specific volume, specific volume of the injected water, wellbore diameter, and reservoir flow and storage capacities. For the line source solution, skin factor is an additional input parameter, while for the vertical fracture solution, the length of the vertical fracture intersecting the wellbore is an additional input parameter.

The pressure behavior calculated from the model is then compared with the observed pressure behavior. If the simulated pressure and observed pressure behaviors agree within a chosen tolerance, the behavior of the well is assumed to be matched. That is, the assumed model with the chosen parameters is considered to be calibrated. If the calculated and observed pressure behaviors do not match, one or more of the input parameters to the model are changed and the pressure behavior is recalculated. The trial-and-error process is continued until the calculated pressure behavior matches the observed within the tolerance chosen based on the sensitivity and accuracy of the pressure measurements. Once the match is obtained, the hydrologic properties used to achieve the match can be considered to be reasonable estimates for the reservoir.

Analysis Results

Figure 3 presents the match between the calculated and measured pressures using the line source solution. The pressures for the step-rate test and fall-off test were taken with the TPS tool set at different depths; 6,000 feet and 4,201 feet, respectively. In Figure 3 these measured pressures have been normalized to a common datum, equivalent to an initial static pressure of 1,500 psia. The match in Figure 3 required reservoir flow capacity and storage capacity values of 4,000 millidarcy-feet (md-ft) and 0.001 ft/psi, respectively; both these values are very low, confirming the non-commercial nature of this well. The Desert Peak hydrothermal reservoir, about 1.5 mile west of this well, has much higher

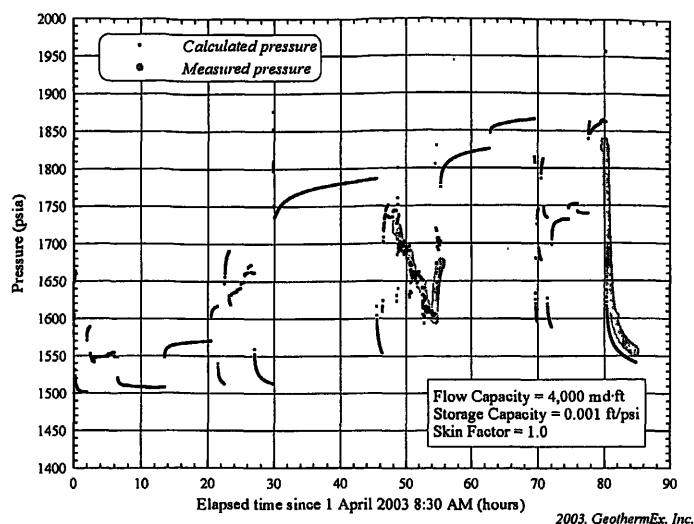


Figure 3. Pressure history match using line source solution.

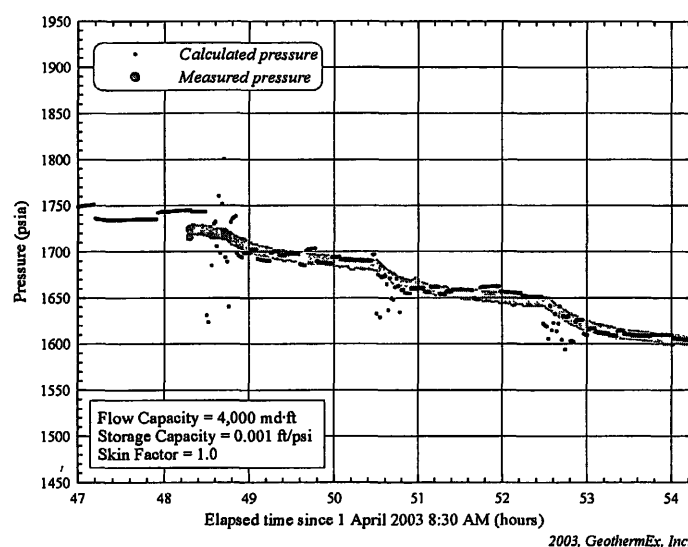


Figure 4. Pressure history match using line source solution.

flow and storage capacities: 33,000 to 423,000 md-ft and 0.003 to 0.007 ft/psi, respectively (Goyal *et al.*, 1983).

The match in Figure 3, for a skin factor of 1, appears good during the step-rate test period, but deteriorates immediately afterwards. It appears that the skin factor declined to -0.2 (that is, the well improved in injectivity slightly) following the three-step rate test. This improved injectivity can be correlated with the sudden spike in injection rate observed after an elapsed time of 54.3 hours (Figure 2); it is tempting to speculate that the sudden increase in injection cleaned up some clogged fractures, improving injectivity. Figure 4 shows the details of the match obtained between calculated and measured pressures during the three-step rate test (assuming a skin factor of 1). Figure 5 shows the details of the match (assuming a skin factor of -0.2) for the period following the three-step rate test. The matching discussed above assumed a well producing from a porous medium with a skin factor, which could reflect a combination of wellbore damage and “incomplete penetration”. This latter effect could be caused by the fact that,

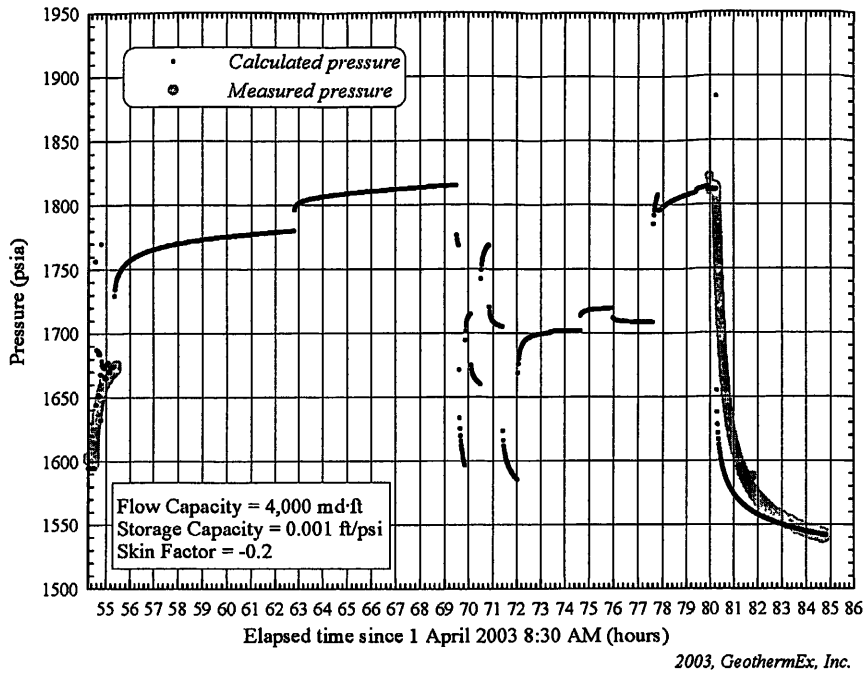


Figure 5. Pressure history match using line source solution.

of the more than 5,000 feet of open interval in the well, TPS logs indicate that less than half takes any injection water (Figure 1).

To confirm that the well did not intersect a major fracture (which, given the geologic setting, is most likely to be steeply-dipping), the above matching process was repeated using the vertical fracture solution. For the three-step rate test, as close a match between calculated and measured pressures as in Figure 5 could be achieved using the uniform-flux vertical fracture solution. In this case the flow capacity had to be lowered to 2,600 md-ft but the storage capacity was held the same; the fracture length required for this match was only 6 feet. For the period following the three-step rate test, calculated and measured pressures could be matched using the uniform-flux vertical fracture solution for the same storage capacity and a flow capacity of 2,600 md-ft,

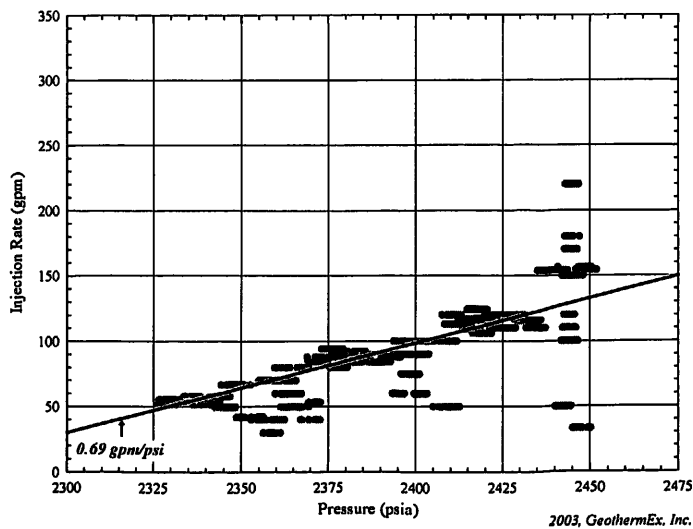


Figure 6. Step-rate test pressures vs. injection rate.

but the fracture length needed to be increased to 8 feet. As in the case of the line-source solution, trial-and-error matching of calculated and measured pressures indicates an increase in injectivity following the injection rate spike at 54.3 hours. These small estimated fracture lengths imply that, for all practical purposes, the well does not intersect any major fracture.

Considering that the total rock-fluid compressibility in such geothermal systems is typically on the order of 10^{-5} psi⁻¹ and the open interval in the well is at least 5,000 feet, the low storage capacity value (0.001 ft/psi) estimated signifies a very low average reservoir porosity (on the order of 2%). The radius of investigation during the 80-hour injection test was calculated to be 1,440 feet.

Figure 6 is a plot of the measured injection rate versus pressure (at 6,000 ft depth) during the three-step rate test. A linear fit to the data indicates an injectivity index of 0.69 gpm/psi. This level of injectivity is extremely low compared to the injectivity of typical geothermal injection wells, reflecting the low flow capacity of the reservoir. Since the skin factor had decreased slightly after the three-step rate

test, the injectivity was estimated to have increased from 0.69 to 0.8 gpm/psi.

Methodology for Assessing Stimulation Results

Assessment Approach

Injection testing described above has defined the background condition against which the results of future stimulation of well DP 23-1 (in Phase II of the project) can be assessed. One approach to quantification of the stimulation results would be to conduct geophysical investigations on the ground surface or in the wellbore after stimulation to define the extent and geometry of the stimulated zone and to characterize the fractures. But such definitions are not readily correlatable to the practical aspects of wellbore hydraulics. Therefore, we propose to assess the effectiveness of stimulation through simple injection tests, from which the transmissivity and volume of the stimulated reservoir can be estimated readily. In addition, the proposed methodology will allow the quantification of other beneficial aspects of wellbore stimulation: reduction in skin factor, increase in length of any fracture intersecting the well, and augmentation of the injectivity index. The methodology presented below would allow a rapid, low cost and approximate assessment of the success of hydraulic stimulation in Phase II. This preliminary assessment could then be followed by geophysical investigations, other reservoir tests, and numerical reservoir modeling, as deemed appropriate.

Proposed Methodology

The methodology consists of 3 steps as follows:

1. Conduct a short-term injection test involving several rate steps of several hours duration each. Measure the downhole pressure

continuously during the step-rate test and for several hours during pressure fall-off following the stoppage of injection. Estimate the injectivity index from the rate and pressure data; the higher this estimate compared to the pre-stimulation value, the more successful the stimulation.

- From either the step-rate test or fall-off test, or both, estimate the reservoir flow capacity and wellbore skin factor using the methodology described before. The success of stimulation would be indicated by the extent of increase in flow capacity and decrease in skin factor. An increase in injectivity due mainly to a decrease in skin factor would imply stimulation of the near-wellbore region only, while increased injectivity due primarily to an increase in reservoir flow capacity would reflect the creation of an artificially fractured reservoir of significant volume. Obviously, the latter situation is more attractive from the viewpoint of an EGS project.

If the measured and calculated pressure behaviors can be better matched by invoking a vertical fracture solution, estimate the length of the vertical fracture; the longer the vertical fracture compared to its pre-stimulation length, the more successful the stimulation. For an EGS project, the creation of a significant fractured reservoir volume around the well would be more attractive than the opening or extension of a single major fracture at the well.

- Unless stimulation results in the conspicuous creation or extension of a single major fracture, conduct a long-term (several weeks) injection test at a relatively constant rate and use either of the following approaches to estimate the transmissivity and radius of the stimulated area around the well. The two alternative approaches, as described further in the Appendix, would allow cross-checking of the results to ensure accuracy:

- Type-curve matching (Bixel and Van Poolen, 1966): In this approach a pseudo-dimensionless pressure, calculated from the measured pressure increase is plotted against time on a semi-log paper and the resulting data point trends are matched to one of a set of type-curves (Figure 7). From this match, the transmissivity and radius of the stimulated zone can be estimated.

- Semi-log plotting (Odeh, 1969): In this approach the pressure increase versus time is plotted on a semi-log paper and the slopes of an expected initial linear trend as well as a later linear trend in data points are estimated. Figure 8 schematically illustrates such a plot. From these slopes and the point of intersection of the two linear trends, it is possible to estimate the transmissivity and radius of the stimulated zone.

Potential Limitations

If the injection test has not been run long enough to achieve a radius of investigation several times larger than the radius of the stimulated zone, the latter cannot be estimated. To avoid this limitation, the test should be continued until the gathered data match one of the type-curves in Figure 7 or develop the second linear trend as shown in Figure 8. Even if the second linear trend does not develop after the initial linear trend has clearly ended,

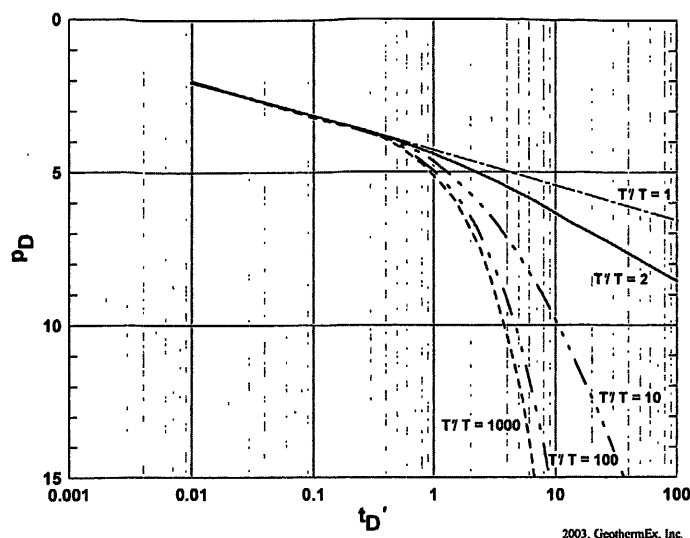


Figure 7. Type curves for pressure drawdown behavior after well stimulation (after Bixel and Van Poolen, 1967).

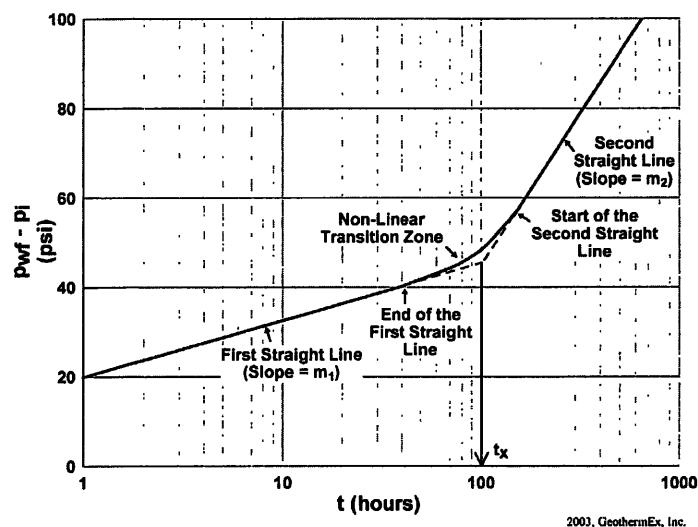


Figure 8. Schematic injection pressure vs. time behavior of a stimulated injection well.

an approximate value of the radius of the stimulated volume can be calculated from equation (A-10) in the Appendix.

Transmissivity is a function of both the flow capacity of the reservoir and the viscosity of the fluid. For Steps 1 and 2 of the methodology, the short duration of injection will not cause significant cooling in the reservoir, and therefore, flow capacity can be calculated from the estimated transmissivity by using the fluid viscosity at the original reservoir temperature. On the other hand, if the test needs to be run for an unduly long time in order to ensure a sufficiently large radius of investigation compared to the radius of the stimulated zone, a significant portion of the reservoir around the wellbore may be cooled. In such a case, calculation of flow capacity from the estimated transmissivity may be compromised by the uncertainty in fluid viscosity (lying somewhere between the viscosity values at the injection temperature and reservoir temperature). Fortunately, this is unlikely to be a significant limitation for most stimulation cases.

Conclusions

1. The wellbore could be cooled down by water injection to allow successful running of the wellbore imaging log.
2. The injection required for wellbore cooling was successfully utilized for a step-rate injection test as well as a pressure fall-off test.
3. Analysis of the injection test results confirms that the reservoir has very low flow capacity (4,000 millidarcy-feet) and the well does not intersect a major fracture.
4. The well has a very low injectivity index (0.69 gpm/psi), which improved slightly (to 0.8 gpm/psi), the apparent skin factor decreasing (from 1 to -0.2) after 54.3 hours of injection.
5. The skin factor appears to be a combination of wellbore damage and incomplete penetration (less than half of the 5,000-foot open interval taking injection water).
6. The low storage capacity (0.001 ft/psi for a 5,000-foot open interval) estimated from the injection test implies a very low reservoir porosity (on the order of 2%).
7. The flow and storage capacities at this well are far lower than encountered within the known hydrothermal reservoir at Desert Peak.
8. The injection testing established the baseline condition against which the efficacy of planned reservoir stimulation (increase in injectivity, flow capacity and/or fracture length; reduction in skin factor; and volume of the stimulated zone) can be

judged using a practical, low cost, approximate methodology proposed here.

Acknowledgements

The authors gratefully acknowledge the support for this project from the U.S. Department of Energy, Assistant Secretary for Energy Efficiency and Renewable Energy, under DOE Idaho Operations Office Financial Assistance Award DE-FC36-02ID14406. We also thank Alex Schriener of Earthrock Consulting for his insightful critique of this paper, and the operating staff of ORMAT for their assistance in conducting field operations.

References

- Bixel, H. C. and H. K. Van Poolen, 1966. "Pressure Drawdown and Buildup in The Presence of Radial Discontinuities." *AIME Transactions*, 240.
- Earlougher, R. C., 1977. "Advances in Well Test Analysis." Henry L Doherty Series, Society of Petroleum Engineers. Monograph Volume 5.
- Goyal, K. P., W. R. Benoit, J. P. Mass, and J. R. Rosser, 1983. "Desert Peak: A Geothermal Field in Churchill County, Nevada." Ninth Workshop on Geothermal Reservoir Engineering *Proceedings*.
- Gringarten, A. C., H. J. Ramey, Jr., and R. Raghavan, 1975. "Applied Pressure Analysis for Fractured Wells." *AIME Transactions*, 259.
- Odeh, A. S., 1969. "Flow Test Analysis for a Well with Radial Discontinuity." *Journal of Petroleum Technology*.
- Robertson-Tait, A. and C. Morris, 2003. "Progress and Future Plans at The Desert Peak EGS Project." Submitted for Presentation at the Annual Meeting of the Geothermal Resources Council, October, 2003.

APPENDIX

Estimating Radius of the Stimulated Area

Type-Curve Matching

Figure 7 presents a set of "type curves" showing a dimensionless pressure (p_D) versus a dimensionless time (T_D) following the approach of Bixel and Van Poolen (1966):

$$p_D = \frac{T'}{141.2q} (p_{wf} - p_i) \text{ and} \quad (\text{A-1})$$

$$t_D = 0.0002636 \left(\frac{T'}{S} \right) \left(\frac{t}{a^2} \right) \quad (\text{A-2})$$

where p_{wf} is flowing pressure (psi), and p_i is initial pressure (psi), q is volumetric injection rate in reservoir condition (barrels/day), t is time (hours), a is radius (ft) of the stimulated zone around the well, T' is transmissivity within the stimulated zone (md-ft/cp), and S is storage capacity (ft/psi). Transmissivity is defined as:

$$T' = \frac{(kh)'}{\mu}, \quad (\text{A-3})$$

where $(kh)'$ is flow capacity (md-ft) in the stimulated zone. Figure 7 makes the reasonable assumption that the storage capacity

remains essentially unchanged by stimulation. In Figure 7 the type curves are shown for a range of the ratio of stimulated-to-original transmissivity (T). The type curves can be used as proposed below.

Plot the calculated values of p_D (using equation A-1 and the value of T' estimated from Step 2) versus time on a tracing paper overlain on Figure 7 such that the semi-log plot of measured p_D versus time and the type-curves have the same scales for both the abscissa and the ordinate. Shift the overlain data plot keeping the axes parallel to those of Figure 7 until the data points match one of the curves in Figure 7. Once this match is obtained, choose any point on the data plot and note its t (hours) coordinate and the t_D coordinate of the corresponding point on Figure 7 underneath. Substitute these values in (A-2) to calculate the radius (a) of the stimulated volume. The S value for (A-2) is the same as estimated before (0.001 ft/psi).

Semi-Log Plotting

Plot the pressure increase versus dimensionless time (t_D) during the long-term test on a semi-log plot as shown schematically in Figure 8, t_D being defined as:

$$t_D = 0.0002636 \left(\frac{T'}{S} \right) \left(\frac{t}{r_w^2} \right) \quad (\text{A-4})$$

The data points should define an initial linear trend of slope m_1 , followed by a later linear trend of slope m_2 (if the test has been of sufficient duration) with a non-linear transition zone in between. The slope of the first line can be used to calculate the transmissivity of the stimulated zone:

$$T' = \frac{162.6q}{m_1}, \quad (\text{A-5})$$

This T' value should be the same as calculated in Step 2 unless prolonged injection has further altered the transmissivity initially achieved by stimulation. Similarly, the slope of the second line can be used to calculate the original transmissivity (T) of the reservoir beyond the stimulated volume:

$$T = \frac{162.6q}{m_2} \quad (\text{A-6})$$

This T value should be close to 4,000 md-ft estimated before. When the second linear trend develops, define the point of intersection of the two linear trends by extrapolation, and note the time value (t_x) for this point (Figure 8). Calculate the dimensionless time (t_{DX}) corresponding to t_x using (A-4).

The radius of the stimulated zone has been correlated to t_{DX} (Odeh, 1969) as:

$$\frac{a}{r_w} = \left[\frac{2.25t_{DX}}{M^{M(M-1)}} \right]^{1/2}, \quad (\text{A-7})$$

$$\text{where } M = T' / T \quad (\text{A-8})$$

and r_w = wellbore radius (ft).

$$\text{From (A-5) and (A-6), } M = m_2/m_1 \quad (\text{A-9})$$

The calculation above can then be verified as follows. Odeh (1969) showed that the first straight line should end at a dimensionless time given by:

$$\frac{a}{r_w} = (6.7t_D)^{1/2}, \quad (\text{A-10})$$

and the second line should start at a dimensionless time given by:

$$\frac{a}{r_w} = \left(\frac{0.13t_D}{M} \right)^{1/2}. \quad (\text{A-11})$$

Therefore, once the value of a/r_w has been determined from (A-7), the end of the first linear trend and start of the second linear trend can be estimated from (A-10) and (A-11), respectively. These estimates can then be checked against the semi-log plot (Figure 8) to ensure correct calculation of the value of a .

A

Abe, J. 303
Adachi, M. 827
Akin, Serhat 811
Alam, M. A. 81
Alexander, James H. 801
Allis, R. 249, 319
Almanza, Rafael 543
Alvarez Rosales, Julio 377
Amistoso, A. E. 765
Antal, Cornel 89
Anthony, Elizabeth Y. 639
Aragón-Aguilar, A. 131, 679
Arehart, Greg B. 269
Arellano G., V. M. 275, 281, 307, 679
Arias, A. 755
Asanuma, Hiroshi 349, 689

B

Baria, Roy 349
Barnett, P. 209
Barragán, R. M. 275, 281, 679
Barrios, L. 755
Barton, Colleen 879
Batini, F. 261
Bennett, Richard A. 3
Berard, Brian 879
Bertani, R. 755
Berndt, M. L. 125
Bignall, G. 303, 369
Birkle, P. 287
Blackwell, D. D. 21, 33
Blewitt, Geoffrey 3, 9
Bloomfield, Kit 383, 593
Bour, Daniel L. 147, 163
Bourcier, William L. 519
Boyd, Tonya L. 77
Briseño, Eduardo Reyes 477
Brophy, Paul 293
Brown, P. J. 885
Bruton, Carol J. 519
Burton, Elizabeth A. 519

C

Calvin, Wendy 653, 673
Camacho Hernández, J. M. 377
Canchola Félix, Ismael 523
Ceccarelli, A. 755
Chandrasekharam, D. 81
Chen, Chih-Ying 793
Christensen, Chelsea 249

Ciulli, B. 261
Clark, James R. 331
Climaco, Juan M. 155
Cobo-Rivera, Juan M. 833
Cocks, P. A. 657, 673
Contreras, Juan 473
Coolbaugh, Mark F. 3, 9, 269, 653

D

Darnet, Mathieu 355
Davis, James L. 3
de Henríquez, Elizabeth C. 213
de León Vivar, Jesús 685
De Matteis, R. 261
Delattre, M. 527
Detwiler, Russell L. 359
Dickens, James 583
Dini, I. 755
DiNicola, Tony 497
Dong, Bin 547
Dudley-Murphy, Elizabeth A. 645
Duffield, Wendell 629
Dulce, Rosella G. 467
Dunlevy, Paul 419

E

Elders, Wilfred A. 423
Ellis, Richard 33
Entingh, Daniel J. 533
Espinosa-Paredes, G. 131
Espinoza, Emigdio Casimiro 85
Evangelista, Raul 503

F

Farhar, Barbara C. 419
Faulds, James E. 859
Felger, Tracey 629
Fernandez, Noel A. 485
Fikre-Mariam, A. 209
Finger, John T. 169, 197
Fiordelisi, A. 261, 755
Flores, Carlos 219
Fomin, S. 747
Foxall, William 673
Fragata, Jimmy J. 503
Fridleifsson, Guðmundur O. 423
Fujiwara, Hiroshi 69

G

García-Gutiérrez, A. 131, 679
Garibaldi, Fortunato 477

García-Estrada, Gerardo 603, 609
Garg, Sabodh K. 801, 841
Garside, Larry 27, 859
Gastineau, John 147
Gavrilescu, Ovidiu 89
Gawlik, Keith 577
Gilbert, Chris 761
Glowacka, Ewa 473
Goko, K. 827
González, Carlos 177
González, R. 281
González, William J. 477
Gordan, Mircea 89
Goyal, Keshav 383
Gritto, Roland 223
Grossman, James W. 197
Guidotti, Ronald A. 173
Gutiérrez-Negrín, Luis C.A. 53

H

Haizlip, Jill 293
Hamza, V. M. 59, 615
Handal, S. 755
Hashida, T. 747
Hassani, Vahab 583
Hatakeyama, Kazuyoshi 807
Hayashi, Kazuo 689, 695
Hays, Lance 539, 571
Henneberger, R. C. 885
Helm-Clark, Catherine M. 15
Hernández, J. 281
Hernandez, Rafael 163
Hernández Morales, David 137
Hernández Soria, S. S. 523
Hill, Roger 449
Hirano, N. 303
Hirsch, Steve 429
Hodgson, Susan Fox 93
Holt, William 3
Hoover, Eddie R. 169
Horne, Roland N. 707, 715, 793
Hulen, Jeff 227, 383

I

Iglesias, Eduardo R. 619
Ishido, T. 807, 827, 841, 847, 851
Ishizaki, J. 827
Ito, Shin 689
Ito, Takatoshi 695
Itoi, Ryuichi 387
Ivan, Catalin 155
Izquierdo M., Georgina 307, 679
Izumi, Tanemoto 349

J

Jacobs, Gregory 43
 Jacobson, Ronald D. 197
 Jaimes-Maldonado, J. Guillermo 699
 Ji-Yang, Wang 65
 Jialing, Zhu 97
 Johnson, Glenn W. 663
 Johnson, Stuart D. 547
 Jones, Rob 349
 Jotaki, Hisashi 245

K

Kajiwara, Tatsuya 851
 Kamei, Junko 387
 Karingithi, Cyrus W. 311
 Kasameyer, Paul 673
 Kaspereit, Dennis 227
 Kasteler, Christian 403
 Kellogg, Norman L. 477
 Kennedy-Bowdoin, T. 649, 673
 Kitao, Koji 183
 Knudsen, Steven D. 197
 Kovac, Katie 879
 Kovscek, Anthony R. 811
 Kozubal, Eric 587
 Kratt, Chris 653
 Kun, Wang 393
 Kutscher, Charles 587

L

Lahsen, Alfredo 635
 Lawless, J. V. 433, 761
 Leif, Roald 519
 Lentz, Alvaro 543
 Li, Kewen 707, 715, 771, 793
 Lichti, Keith A. 485, 503
 Lima Lobato, Enrique Manuel 69
 Lin, Mow S. 547
 Lippmann, M. J. 335
 Listi, Renan 47
 López, D. L. 325
 López, Raúl Edgardo 491
 López-Hernández, Aída 603, 609
 Louie, John N. 9
 Lovekin, J. W. 885
 Lovelock, B. G. 433
 Lozada, R. 275
 Lund, John W. 101
 Lutz, Susan Juch 865

M

Mac Knight IV, Robert B. 673

Magaña, M. I. 325
 Maghiar, Teodor 89
 Majer, Ernest L. 223
 Malate, R. C. M. 765
 Mancini, C.E. 125
 Mansure, Arthur J. 141, 197
 Marocco, B. M. 755
 Marquis, Guy 355
 Marrero, R. 325
 Martínez, J. 281
 Martini, B. A. 649, 657, 673
 Martinović, Mića 241
 Matsunaga, Isao 785
 Matsuzaki, Ryo 387
 Matthews, Oliver 197
 McCulloch, Jess 147, 879
 McKenn, J. R. 21
 McFee, Jason 711
 McVeigh, James F. 533
 Mella, Mike 403
 Melosh, Glenn 497
 Meziani, M. 527
 Milivojević, Mihailo 241
 Mines, Greg 593, 597
 Mink, Roy 439
 Minor, Timothy B. 9
 Miyairi, Makoto 737
 Mizunaga, Hideki 245
 Mohr, C. 593
 Momita, Manabu 69
 Mongillo, M. A. 443
 Montaña, Jorge 623
 Monterrosa, M. 755
 Moore, J. N. 249, 319, 879
 Mora, Othon 477
 Morgan, Paul 629
 Morris, Christy 871, 885
 Mouché, Richard J. 43
 Moya, Paul 177, 551
 Murray, Brad 249
 Murray, Larry 227
 Mustopa, Enjang Jaenal 245

N

Nakao, Shinsuke 807
 Nakatsuka, K. 111
 Nash, G. D. 645, 663, 669, 673
 Nemčok, Michal 249
 Nieva, David 443
 Niitsuma, Hiroaki 349, 689
 Nikolski, Alexander I. 557
 Nishi, Yuji 827, 847
 Noello, Eduardo 155
 Nogara, James B. 467
 Norman, D. 319

Normann, Randy A. 173
 Norton, Denis 227
 Norwood, Susan 449

O

Oakley, Doug 155
 Odinek, Judy 173
 Ogryzlo, C. T. 433
 Ohsaki, Yutaka 737
 Okada, Wataru 761
 Omenda, Peter A. 639
 Oppliger, Gary L. 9, 859
 Orizonte, Jr., R. G. 765
 Ouma, Peter A. 397

P

Padrón, E. 325
 Paiuk, Benjamin 155
 Pal, Dharminder 669
 Peel, Elena 623
 Pelant, Frank G. 477
 Pérez, A. 335
 Pérez, Diego 551
 Pérez, N. M. 325
 Philippacopoulos, A. J. 125
 Pickles, W. L. 649, 657, 673
 Portugal M., Enrique 281, 307
 Potts, Donald C. 673
 Poulson, Simon R. 269
 Povarov, Konstantin O. 557
 Povarov, Oleg A. 557
 Powell, Tom 771
 Premuzic, Eugene T. 547
 Pritchard, Wyatt A. 197
 Pritchett, John W. 801, 841
 Pruess, Karsten 817

Q

Quezada, A. 755
 Quijano-León, José Luis 53

R

Raines, Gary L. 9
 Ramírez-Hernández, Jorge 833
 Ramos, Sylvia G. 503
 Randle, J. B. 209, 433
 Rangel-German, Edgar R. 811
 Ravi, Kris 147
 Raymond, Jasmin 331
 Reinhardt, Frederick W. 173
 Renner, J. L. 15
 Reyes, Jericho L. P. 715

Reyes-López, Jaime A. 833
Rivas, José 365
Roberts, Jeffery J. 359
Robertson-Tait, Ann 865, 871, 885
Rodríguez, Carlos 155
Rodríguez, M. H. 335
Rodríguez R., Marco H. 779
Rose, Peter E. 403, 879
Rosell, Josephine B. 503
Rubin, Danilo D. 503
Rybach, Ladislaus 115

S

Saeki, Kazuhiro 183
Saito, Seiji 183
Salgado, Anthony 43
Sánchez V., Eduardo 107
Sánchez-Velasco, R. A. 453, 539,
571, 699
Sandoval, F. 275, 281
Santini, Paolo 565
Santos, P. 755
Santoyo-Gutiérrez, E. 131
Santoyo-Gutiérrez, S. 131
Sanyal, S. K. 885
Sarytchikhina, Olga 473
Sass, John 629
Sawatzky, Don L. 3, 9
Scandiffio, G. 755
Schochet, Daniel 865, 885
Schriener Jr., Alexander 865
See, Fidel S. 503
Sekine, Kotaro 369, 695
Sepúlveda, Fabián 635
Sheridan, Judith 879
Serpen, Umran 459
Shevenell, Lisa 9, 27
Shimada, Kanichi 69
Shook, G. Michael 407
Silva Dias, F. J. S. 615

Silver, E. A. 649, 657, 673
Smith, Richard P. 15
Sohal, Manohar 597
Sonnenthal, Eric 817
Spielman, Paul 413, 879
Spycher, Nicolas 817
Stark, Mitch 727
Stevens, Jeffry L. 841
Suárez Arriaga, Mario César 733
Sugama, Toshifumi 577
Sugita, Hajime 785
Suto, Yuko 111, 183
Swenson, Daniel 695

T

Takahashi, Yoshinobu 737
Tanaka, Toshiaki 387
Tao, Hiroaki 785
Terzaghi, Sergei 761
Tezuka, Kazuhiko 737
Tessari, Robert M. 189
Togo, Hiroshi 69
Tomarov, Grigori V. 557
Torres, M. A. 275
Torres, Rodolfo 365, 619
Tosha, T. 827, 841, 847
Truesdell, A. H. 335
Tsuchiya, N. 111, 303, 369, 743
Tüfekçioğlu, Haluk 459
Tuttle, John D. 47

U

Uchida, Toshihiro 255
Ushijima, Keisuke 245
Ussher, Greg 761

V

van de Putte, Todd 227

Vanorio, T. 261
Velador, Jesus M. 639
Vera Cruz, Rolan P. 485
Verduzco, Fernando Samaniego 733
Verma, Mahendra P. 341, 679
Volpi, G. 755

W

Waibel, Albert F. 33, 673
Wallace, Adam 519
Wannamaker, Philip E. 37
Warren, Tommy 189
Watanabe, N. 743
Wei, Zhang 97
Welker, Benjamin 249
Were, Joshua O. 511
Westmoreland, J. J. 141
Williams-Jones, Anthony E. 331
Wise, Jack L. 197
White, Phil 761
Whitehouse, Harper 711
Wright, Melinda 227

X

Xu, Sheng Heng 115
Xu, Tianfu 817

Y

Yanagisawa, Norio 785
Yasukawa, Kasumi 851
Yoshida, K. 747

Z

Zaide-Delfin, Maribel C. 213
Zheng, Xiuhua 119
Zhou, Wei M. 547
Zollo, A. 261